

Degenerate n-Doping of Few-Layer Transition Metal Dichalcogenides by Potassium

Hui Fang,^{†,‡,§} Mahmut Tosun,^{†,‡,§} Gyungseon Seol,^{||} Ting Chia Chang,^{†,‡,§} Kuniharu Takei,^{†,‡,§} Jing Guo,^{||} and Ali Javey^{*,†,‡,§}

[†]Electrical Engineering and Computer Sciences, University of California, Berkeley, California 94720, United States

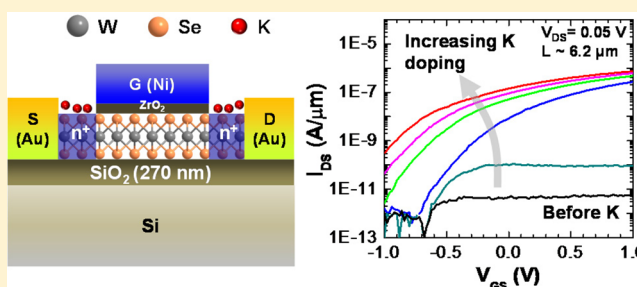
[‡]Materials Sciences Division, Lawrence Berkeley National Laboratory, Berkeley, California 94720, United States

[§]Berkeley Sensor and Actuator Center, University of California, Berkeley, California 94720, United States

^{||}Electrical and Computer Engineering, University of Florida, Gainesville, Florida 32611, United States

ABSTRACT: We report here the first degenerate n-doping of few-layer MoS₂ and WSe₂ semiconductors by surface charge transfer using potassium. High-electron sheet densities of $\sim 1.0 \times 10^{13} \text{ cm}^{-2}$ and $2.5 \times 10^{12} \text{ cm}^{-2}$ for MoS₂ and WSe₂ are obtained, respectively. In addition, top-gated WSe₂ and MoS₂ n-FETs with selective K doping at the metal source/drain contacts are fabricated and shown to exhibit low contact resistances. Uniquely, WSe₂ n-FETs are reported for the first time, exhibiting an electron mobility of $\sim 110 \text{ cm}^2/\text{V}\cdot\text{s}$, which is comparable to the hole mobility of previously reported p-FETs using the same material. Ab initio simulations were performed to understand K doping of MoS₂ and WSe₂ in comparison with graphene. The results here demonstrate the need of degenerate doping of few-layer chalcogenides to improve the contact resistances and further realize high performance and complementary channel electronics.

KEYWORDS: Degenerate doping, few-layer, TMDCs, MoS₂, WSe₂, potassium, surface charge transfer



The desire for enhanced computation power has been the driving force for the aggressive scaling of electronic devices over the past several decades. However, at the extreme channel length miniaturization, poor gate control impairs the scaling benefits of conventional transistors.^{1,2} In this regard, various new classes of materials and device structures have been proposed to continue the scaling trend.^{3–10} Recently, two-dimensional (2D) layered transition metal dichalcogenides (TMDCs), for example, MoS₂ and WSe₂, have gained tremendous interest due to their body thickness scalability down to a monolayer (ML) without surface dangling bonds or native oxides and with promising carrier transport properties.^{8,10} Field-effect transistors (FETs) fabricated from exfoliated TMDC crystals exhibit outstanding device performances such as an ideal subthreshold swing of $\sim 60 \text{ mV}/\text{dec}$, $I_{\text{ON}}/I_{\text{OFF}}$ ratio of 10^8 , and high field effect mobility for both electrons and holes.^{8–11} Transistors fabricated on 5 nm thick MoS₂ flakes show no short channel effects down to a channel length of $\sim 100 \text{ nm}$ without aggressive gate oxide scaling.¹² Shortly after the first successful demonstration of MoS₂ monolayer FETs,⁸ building blocks of digital circuits such as logic gates, static random access memory devices, and ring oscillators have been realized.^{13,14}

Controlled doping of few-layer TMDCs, which is of fundamental material and device importance, has not yet been well explored in the community. This is particularly

important given that TMDC FETs reported so far are often limited by Schottky barriers (SBs) at the metal/semiconductor interfaces.^{10,12,15,16} Therefore electrical properties are hindered by the contact resistances rather than intrinsic material properties. To be able to push TMDC FETs to their performance limits and also reveal their intrinsic electronic transport properties, recently we reported the use of NO₂ molecules as effective p-dopants for monolayer and few-layer WSe₂.¹⁰ In this doping scheme, NO₂ molecules are absorbed on the surface of WSe₂, resulting in surface electron transfer from WSe₂ to NO₂ given the strong oxidizing nature of NO₂ molecules. Building on this concept, here we report the first degenerate n-doping of MoS₂ and WSe₂. Specifically, we use potassium as an efficient surface n-dopant and achieve a high electron sheet density of $\sim 1.0 \times 10^{13} \text{ cm}^{-2}$ in MoS₂ and $2.5 \times 10^{12} \text{ cm}^{-2}$ for WSe₂. We also for the first time demonstrate few-layer WSe₂ n-FETs with electron mobility of $\sim 110 \text{ cm}^2/\text{V}\cdot\text{s}$ by selectively n-doping the metal contact regions with K.

Electron doping by K vapor has been previously applied to carbon nanotubes and graphene.^{17–19} Because of the small electron affinity of K, it is a strong electron donor to most surfaces. Here, to study the doping effects of K on the transport

Received: January 4, 2013

Revised: March 27, 2013

Published: April 9, 2013

properties of TMDCs, back-gated devices made of few-layer MoS₂ and WSe₂ with channel lengths of 0.5–10 μm were first fabricated and systematically studied as a function of doping. The fabrication process starts with the transfer of MoS₂ or WSe₂ layers on a Si/SiO₂ substrate (oxide thickness, $t_{\text{ox}} = 270$ nm) using an adhesive tape,⁸ followed by an acetone wash for 1 h to remove the tape residues. Subsequently source/drain (S/D) metal contacts were formed by lithography, metal evaporation, and lift-off processes. The contacts were annealed at 200 °C for 5 min in Ar. The K doping of few-layer chalcogenides was carried out in a sealed chamber, where the samples/devices were placed ~2–3 cm in distance under the K dispenser (SAES Getters, U.S.A.). The chamber was then pumped and maintained at $\sim 3.5 \times 10^{-5}$ Torr by a turbo pump and a current of 5 A was applied to the K dispenser to initiate the doping process. The dose was controlled by monitoring the device performance in situ as a function of exposure time to the K vapor. For MoS₂, Ni and Au metal contacts were found to give good n-type conduction, which is consistent with literature.¹² Here we choose Ni for simplicity. Figure 1a,c

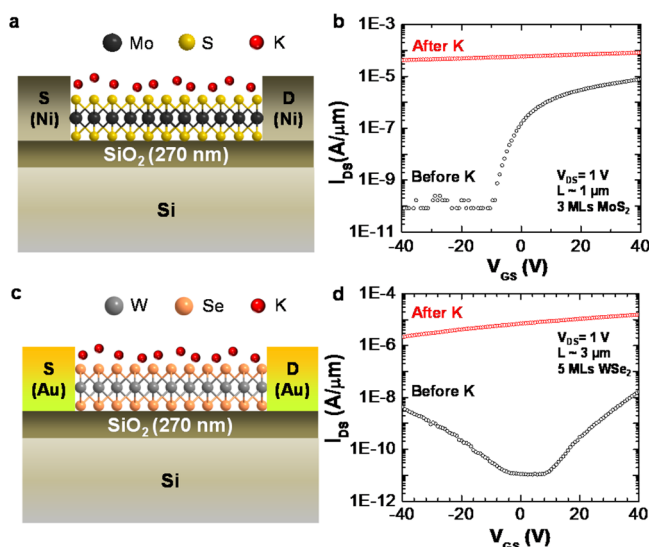


Figure 1. “Blanked” (i.e., unpatterned) n-doping of few-layer MoS₂ and WSe₂ by K. (a,c) The schematic of K doping of the entire channel for MoS₂ and WSe₂ devices, respectively, with (b,d) showing the corresponding transfer characteristics before (black symbols) and after (red symbols) doping.

shows the device schematics of few-layer MoS₂ and WSe₂ back gated FETs blank-doped with K. Figure 1b shows the transfer characteristics of a 3-monolayer MoS₂ back gated device before and after K doping, measured in vacuum. The as-made device exhibits a typical switching behavior with large $I_{\text{ON}}/I_{\text{OFF}}$ ($>10^5$). After doping by exposing the entire channel to K vapor, the current I_{DS} becomes weakly dependent on the gate voltage, which clearly indicates that MoS₂ is heavily n-doped (current at positive bias side still slight higher than negative side). The current level also increases with doping mainly due to two effects: (1) higher tunneling probability through SBs due to barrier thinning by strong doping and (2) higher channel conductance arising from the higher electron concentration. The first effect results in a lower contact resistance and is a more prominent factor given that for as-made devices; the current nearly saturates at very high gate fields (Figure 1b), suggesting that the current is limited by the injection of carriers

from the source contact. For few-layer WSe₂, here we use Au as the contact metal since it results in higher electron conduction (i.e., lower SB height to the conduction band) as compared to the other metal contacts that we explored, including Pd and Ni. Specifically ambipolar device characteristics with both electron (positive V_{GS}) and hole (negative V_{GS}) conduction (Figure 1d) due to the midgap SBs are observed for Au contacted WSe₂ FETs. This is in contrast to Pd contacted FETs which exhibit only p-channel conduction due to lower SBs for holes as compared to electrons.¹⁰ After K doping, WSe₂ FETs also exhibit weak gate dependence in I_{DS} , which coincides with the result from MoS₂, indicating a high electron doping level.

To approximate the sheet electron concentration after K doping, here we assume that K doping results in SB width thinning such that the tunneling probability is near unity. Therefore, the contact resistance after doping can be ignored. The 2D sheet doping concentration ($n_{2\text{D}}$) is then extracted from $n_{2\text{D}} = (I_{\text{DS}}L)/(qWV_{\text{DS}}\mu)$, where q is the electron charge, W and L are the width and length of channel, respectively, I_{DS} is the source/drain current at zero gate voltage, V_{DS} is the source/drain voltage, and μ is the field-effect mobility. The mobility was extracted from the $I_{\text{DS}}-V_{\text{GS}}$ transfer characteristic after doping using parallel plate capacitor model ($C_{\text{ox}} = \epsilon_{\text{ox}}\epsilon_0/T_{\text{ox}}$ is the gate oxide capacitance per unit area, where $\epsilon_{\text{ox}} \sim 3.9$ is the dielectric constant of SiO₂, ϵ_0 is the vacuum permittivity, and $T_{\text{ox}} = 270$ nm is the SiO₂ thickness) to estimate the channel charge modulation. We extract an electron concentration $n_{2\text{D}} \sim 1.0 \times 10^{13}$ cm⁻² for K-doped MoS₂ and 2.5×10^{12} cm⁻² for WSe₂. The difference in the extracted electron concentrations could arise from difference in the K surface coverage for the two samples.

Patterned n-doping of few-layer TMDCs was explored next by fabrication of top-gated few-ML TMDC FETs with self-aligned, K-doped S/D contacts. Specifically, a 3 ML WSe₂ top-gated FET with $L \sim 6.2$ μm is shown here as a proof of concept. Au (40 nm) was used as the S/D contacts. ZrO₂/Ni (17.5/30 nm) gate stack (underlapping the S/D metal contacts by a distance of 300–500 nm) was formed by electron beam lithography, metal deposition and lift-off. To be able to lift off the gate stack, ZrO₂ was deposited by atomic layer deposition (ALD) at a low temperature of ~ 120 °C. Figure 2a depicts the 3 ML WSe₂ top-gated FET after K doping of the exposed S/D. The exposed (underlapped) regions are n-doped heavily, while the gated region remains near intrinsic due to the protection of the active channel by the gate stack. The resulting structure is n⁺/i/n⁺, similar to the conventional n-MOSFETs. Figure 2b shows the transfer characteristics of the device in vacuum with increasing doping time. Here the back-gate voltage is fixed at 40 V to electrostatically dope the underlapped regions. As a result, the difference in the $I_{\text{DS}}-V_{\text{GS}}$ characteristics mainly arises from the change of the metal-WSe₂ contact resistance, rather than the resistance of the underlapped regions. The device before doping shows a low current of <10 pA/μm at $V_{\text{DS}} = 0.05$ V. The electron conduction at the positive gate voltage increases drastically by orders of magnitude after K vapor exposure, which clearly depicts the lowering of the contact resistance. Specifically, the current value after 120 min of doping using the specified condition is $\sim 10^5$ × higher than the device with undoped contacts. Note that a small threshold voltage shift toward the more negative voltage is observed with K doping. This is attributed to the diffusion of a small fraction of the K atoms through the top-gate stack, especially given the small size of K ions.

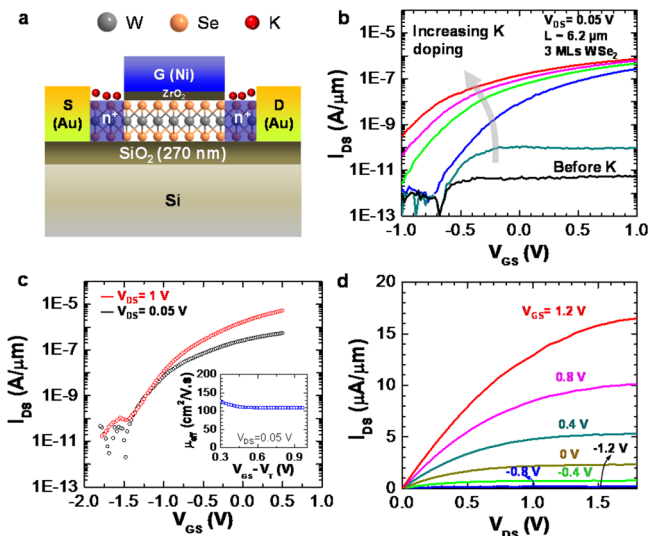


Figure 2. Top-gated few-layer WSe_2 n-FETs with chemically doped contacts. (a) Schematic of a top-gated few-layer WSe_2 n-FET, with chemically n-doped S/D contacts by K exposure. (b) Transfer characteristics of a 3-layer WSe_2 device ($L \sim 6.2 \mu\text{m}$) as a function of K exposure time. The black curve is before doping, while the other curves from bottom to top are after 1, 20, 40, 70, and 120 min doping. (c) Transfer characteristics of the device in (b) after 120 min doping. Inset shows extracted effective electron mobility as a function of the gate overdrive of the device at $V_{\text{DS}} = 0.05 \text{ V}$. (d) Output characteristics of the same device shown in (b).

Figure 2c shows the transfer characteristics of a top-gated WSe_2 FET after 120 min of K doping at both high ($V_{\text{DS}} = 1 \text{ V}$) and low ($V_{\text{DS}} = 0.05 \text{ V}$) fields. The device exhibits $>10^4$ of $I_{\text{ON}}/I_{\text{OFF}}$, and over $110 \text{ cm}^2/\text{V}\cdot\text{s}$ peak effective electron mobility, which was extracted from the I - V characteristics by using the relation $\mu_{\text{eff}} = [(\partial I_{\text{DS}})/(\partial V_{\text{DS}})] [L / (C_{\text{ox}}(V_{\text{GS}} - V_{\text{T}} - 0.5V_{\text{DS}}))]$. Here, $V_{\text{T}} = -0.46 \text{ V}$ is the threshold voltage, V_{GS} is the gate bias and $C_{\text{ox}} = \epsilon_{\text{ox}}\epsilon_0/T_{\text{ox}}$ is the top gate oxide capacitance per unit area ($\epsilon_{\text{ox}} \sim 12.5$ is the dielectric constant of ZrO_2 , ϵ_0 is the vacuum permittivity, and $T_{\text{ox}} = 17.5 \text{ nm}$ is the ZrO_2 thickness). The $I_{\text{DS}}-V_{\text{DS}}$ output characteristic of this device is shown in Figure 2d. The I - V behavior at low V_{DS} region clearly depicts the ohmic contacts, while at high V_{DS} the current saturates by pinch-off, similar to the conventional long-channel MOSFETs.

A similar top-gate device structure was explored for few-layer MoS_2 (Figure 3a). Figure 3b,c shows the $I_{\text{DS}}-V_{\text{DS}}$ output characteristics of a 3 ML MoS_2 top-gated FET with $L \sim 1 \mu\text{m}$ at two different back gate bias V_{BG} , 0 and 40 V respectively. The $I_{\text{DS}}-V_{\text{DS}}$ curves reflect a clear Schottky contact behavior at low V_{DS} regime, even with a back-gate voltage of $V_{\text{BG}} = 40 \text{ V}$ where the underlapped regions are electrostatically doped by the back gate. After K surface charge transfer doping of the underlapped regions, the current goes up by more than 1 order of magnitude at the same V_{BG} (0 V) and top gate bias V_{TG} . Moreover, the Schottky behavior disappears and the low-field regime exhibits an ohmic behavior. The peak effective mobility of this device after K doping of the contacts was extracted to be $\sim 25 \text{ cm}^2/\text{V}\cdot\text{s}$. Note that this mobility value is lower than the highest values previously reported in literature, which may be due to the fact that the top gate dielectric layer was deposited at a low temperature to enable the lift-off process with PMMA resist.

To shed light on the charge transfer between K and TMDCs, X-ray photoelectron spectroscopy (XPS) surface analysis was

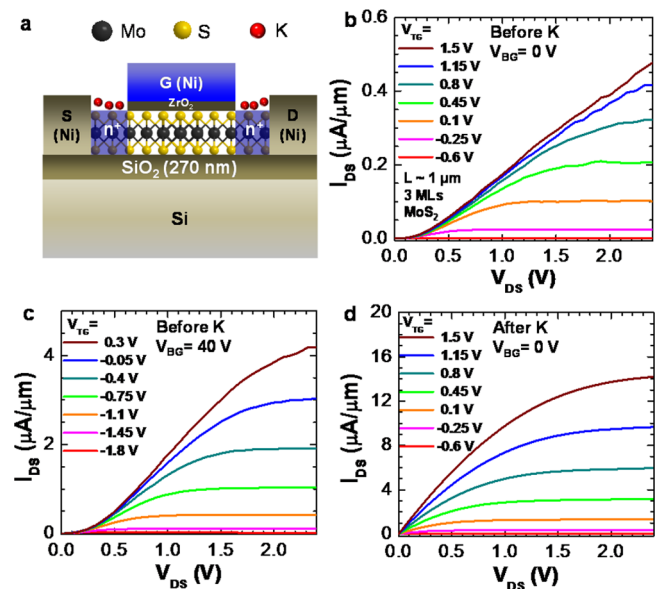


Figure 3. Top-gated few-layer MoS_2 n-FETs with chemically doped contacts. (a) Schematic of a top-gated few-layer MoS_2 n-FET with chemically n-doped S/D contacts by K exposure. (b,c) Output characteristics of a device (thickness of three layers, $L \sim 1 \mu\text{m}$) before K doping at a back gate voltage of 0 and 40 V, respectively. (d) Output characteristics of the same device shown in (b,c) after 120 min of K doping and with 40 V back gate bias.

performed. Figure 4a,b shows the Mo 3d and S 2p peaks, before and after sample exposure to K. After K exposure, the Mo 3d

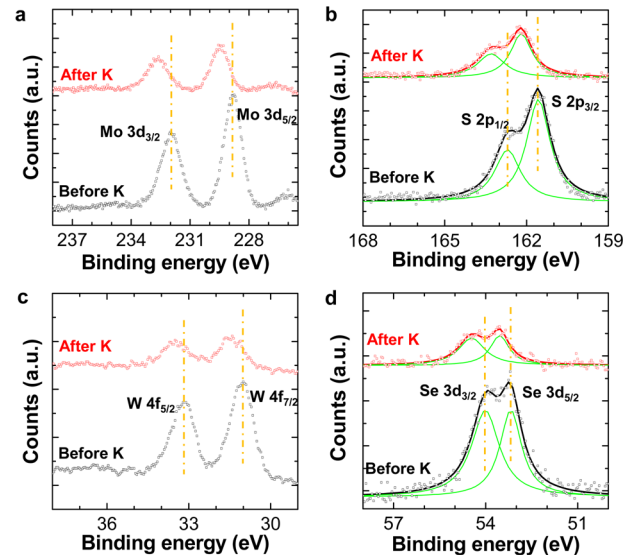


Figure 4. XPS surface analysis of MoS_2 and WSe_2 before and after K doping with binding energy peaks of (a) Mo $3d_{3/2}$ and $3d_{5/2}$, (b) S $2p_{1/2}$ and $2p_{3/2}$, (c) W $4f_{5/2}$ and $4f_{7/2}$, and (d) Se $3d_{3/2}$ and $3d_{5/2}$ electrons. The binding energies at each XPS peak maximum before doping are indicated by the yellow dash lines.

and S 2p peaks broaden while the positions of their maxima shift toward higher values. Specifically, Mo $3d_{3/2}$ shifts from 232.0 to 232.7 eV, Mo $3d_{5/2}$ shifts from 228.8 to 229.5 eV, S $2p_{1/2}$ shifts from 162.7 to 163.3 eV, and S $2p_{3/2}$ shifts from 161.6 to 162.2 eV. The upshift of the peaks is directly attributed to the n-doping process, since it causes a Fermi level shift

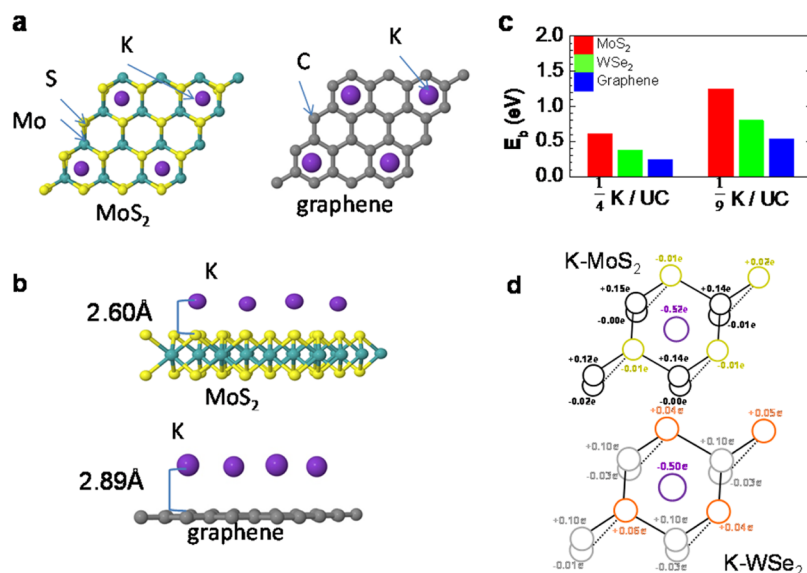


Figure 5. Ab initio simulation of MoS₂ and WSe₂ with binding of K atoms, compared to graphene. (a) Top view and (b) side view schematics of the K-doped MoS₂ and graphene with a doping coverage of 1/4 K atom per unit cell. The distances between K atoms and S or C planes are denoted. The K-doped WSe₂ has a similar structure to that of MoS₂ but with different bond lengths as explained in the text. (c) Binding energy comparison of K–MoS₂, WSe₂, and graphene, with a dopant coverage of 1/4 and 1/9 K atom per unit cell. (d) The change of elemental valence electron distribution of ML MoS₂ (top) and WSe₂ (bottom) after K doping with a coverage of 1/4 K atom per unit cell comparing to before doping.

toward the conduction band edge and the Fermi level is where the zero energy lies. This upshift is also consistent with previous studies of doped graphite and molecular films.^{20,21} Similarly, the peaks of W 4f_{5/2} and 4f_{7/2}, as well as Se 3d_{3/2} and Se 3d_{5/2} upshift (by ~0.4 eV) after K exposure, as depicted in Figure 4c,d. The blue shift of the elemental electron binding energy is a direct indication of the surface charge transfer doping.

Ab initio simulations were performed to further understand the charge transfer and doping mechanism. The simulation was conducted by density-functional theory (DFT) with Vienna ab initio simulation package (VASP) codes,²² and Bader analysis^{23–25} was used to calculate the charge contribution from the potassium dopant.²⁶ Figure 5a,b depicts the top and side view schematics of K-doped MoS₂ and graphene monolayers, respectively, with one side covered with K at a density of 1/4 K atom per unit cell (i.e., one K atom per 4 unit cells). Similar to graphene, the K dopant is located above the centers of the hexagons in MoS₂. Despite of S being a larger atom than C, the distance between the K dopant and the S plane in MoS₂ (2.60 Å) is shorter than that of K and C plane in graphene (2.89 Å). The bond length of K–S is 3.06 Å in MoS₂, compared to the K–C bond length of 3.24 Å in graphene. The shorter bond length indicates a stronger binding of K to MoS₂, which is consistent with a larger binding energy in K-doped MoS₂ and more stable doping as shown in Figure 5c. The simulation results indicate that the bond length decreases and the binding energy increases as the doping density decreases, but the qualitative difference between K-doped MoS₂ and K-doped graphene remains unchanged (Figure 5c). We also performed similar simulations of K–WSe₂. The distance between the K dopant and the Se plane is 2.76 Å and the K–Se bond length is 3.36 Å. Because WSe₂ has larger atoms than MoS₂, the bond length is larger and the binding energy is smaller, but the K–WSe₂ binding energy is still larger than that of K–graphene. To examine charge transfer between the K dopant and ML 2D materials, we performed Bader analysis of charge transfer as

shown in Figure 5d with a K concentration of one atom per four MoS₂ unit cells (as one super cell). After placing one K atom in the center of the super cell, there is 0.52e of charge transferred from the K atom to MoS₂ with the top S atoms sharing the charge, while in ML WSe₂, 0.5 of the K charge is transferred, slightly lower than that of the K–MoS₂ charge. The extracted K doping concentration difference between MoS₂ and WSe₂ from the experimental results in Figure 1b,d is ~4×, larger than the simulation result here. This may be attributed to a number of factors, including difference in the number of K atoms binding to the surfaces for the two materials. Also, it should be noted that the transferred electrons in bonds can be different from the mobile charge carriers due to doping, and the Bader analysis has an uncertainty in determining charge associated with each atom. We also estimated doping density from the simulated density-of-states (DOS) and Fermi energy level. The amount of transferred charge is determined to be 0.55e for K–MoS₂ with a density of 1/4 K per unit cell from the DOS approach, which is consistent with the Bader analysis.

In conclusion, we have studied the surface charge transfer n-doping of few-layer chalcogenides by K. Degenerate doping levels in few-layer MoS₂ and WSe₂ have been achieved and reflected by electrical measurements and surface XPS analysis, and further understood by ab initio calculations. The results here demonstrate the need of degenerate doping of few-layer chalcogenides to improve the contact resistances, and further realize high-performance TMDC channel electronics. Specifically, the work shows that n-type WSe₂ FETs can be obtained with high mobilities that complement those obtained for previously reported p-type WSe₂ FETs¹⁰ by simply doping the contacts accordingly. This finding may enable the development of layered semiconductor CMOS devices in the future. While K is used as a model surface charge transfer dopant in this work, in the future exploration of air-stable dopants is needed.

AUTHOR INFORMATION

Corresponding Author

*E-mail: ajavey@eecs.berkeley.edu.

Notes

The authors declare no competing financial interest.

ACKNOWLEDGMENTS

This work was funded by the Director, Office of Science, Office of Basic Energy Sciences, and Division of Materials Sciences and Engineering of the U.S. Department of Energy under Contract No. De-Ac02-05Ch11231 and the Electronic Materials (E-Mat) program. The device fabrication part of this work was partially supported by NSF E3S Center. A.J. acknowledges support from the World Class University program at Suncheon National University. The work in UF was funded by NSF.

REFERENCES

- (1) Lundstrom, M. *Science (N. Y.)* **2003**, *299*, 210–211.
- (2) Taur, Y. *IBM J. Rev. Dev.* **2002**, *46*, 213–222.
- (3) Choi, Y.; Asano, K.; Lindert, N.; Subramanian, V.; King, T.; Bokor, J.; Hu, C.; Sciences, C. *IEDM Tech. Dig.* **1999**, 919–921.
- (4) Huang, X.; Lee, W.-C.; Kuo, C.; Hisamoto, D.; Kedzierski, J.; Anderson, E.; Takeuchi, H.; Asano, K.; Subramanian, V.; Bokor, J. *IEDM Tech. Dig.* **1999**, 67–70.
- (5) Heyns, M.; Tsai, W. *MRS Bull.* **2009**, *34*, 485–492.
- (6) Luisier, M.; Lundstrom, M.; Antoniadis, D. A.; Bokor, J. *IEDM Tech. Dig.* **2011**, 251–254.
- (7) Ko, H.; Takei, K.; Kapadia, R.; Chuang, S.; Fang, H.; Leu, P. W.; Ganapathi, K.; Plis, E.; Kim, H. S.; Chen, S.-Y.; Madsen, M.; Ford, A. C.; Chueh, Y.-L.; Krishna, S.; Salahuddin, S.; Javey, A. *Nature* **2010**, *468*, 286–289.
- (8) Radisavljevic, B.; Radenovic, a; Brivio, J.; Giacometti, V.; Kis, A. *Nat. Nanotechnol.* **2011**, *6*, 147–150.
- (9) Kim, S.; Konar, A.; Hwang, W.-S.; Lee, J. H.; Lee, J.; Yang, J.; Jung, C.; Kim, H.; Yoo, J.-B.; Choi, J.-Y.; Jin, Y. W.; Lee, S. Y.; Jena, D.; Choi, W.; Kim, K. *Nat. Commun.* **2012**, *3*, 1011.
- (10) Fang, H.; Chuang, S.; Chang, T. C.; Takei, K.; Takahashi, T.; Javey, A. *Nano Lett.* **2012**, *12*, 3788–92.
- (11) Lembke, D.; Kis, A. *ACS Nano* **2012**, *6*, 10070–10075.
- (12) Liu, H.; Neal, A. T.; Ye, P. D. *ACS Nano* **2012**, *6*, 8563–8569.
- (13) Wang, H.; Yu, L.; Lee, Y.-H.; Shi, Y.; Hsu, A.; Chin, M. L.; Li, L.-J.; Dubey, M.; Kong, J.; Palacios, T. *Nano Lett.* **2012**, *12*, 4674–4680.
- (14) Radisavljevic, B.; Whitwick, M. B.; Kis, A. *ACS Nano* **2011**, *5*, 9934–9938.
- (15) Qiu, H.; Pan, L.; Yao, Z.; Li, J.; Shi, Y.; Wang, X. *Appl. Phys. Lett.* **2012**, *100*, 123104.
- (16) Kang, J.; Sarkar, D.; Liu, W.; Jena, D.; Banerjee, K. *IEDM Tech. Dig.* **2012**.
- (17) Kong, J.; Zhou, C.; Yenilmez, E.; Dai, H. *Appl. Phys. Lett.* **2000**, *77*, 3977–3979.
- (18) Javey, A.; Tu, R.; Farmer, D. B.; Guo, J.; Gordon, R. G.; Dai, H. *Nano Lett.* **2005**, *5*, 345–348.
- (19) Ohta, T.; Bostwick, A.; Seyller, T.; Horn, K.; Rotenberg, E. *Science (N. Y.)* **2006**, *313*, 951–954.
- (20) Caballero, A.; Fernfindez, A.; Soriano, L.; Gonzalez-Elipse, A. *Surf. Sci.* **1996**, *364*, 253–265.
- (21) Mahns, B.; Roth, F.; Knupfer, M. *J. Chem. Phys.* **2012**, *136*, 134503.
- (22) Kresse, G.; Furthmuller, J. *Phys. Rev. B* **1996**, *54* (16), 11169–11186.
- (23) Henkelman, G.; Arnaldsson, A.; Jónsson, H. *Comput. Mater. Sci.* **2006**, *36*, 354–360.
- (24) Sanville, E.; Kenny, S. D.; Smith, R.; Henkelman, G. *J. Comput. Chem.* **2007**, *28*, 899–908.

(25) Tang, W.; Sanville, E.; Henkelman, G. *J. Phys.: Condens. Matter* **2009**, *21*, 084204.

(26) For the simulation, the double- ζ polarized (DZP) basis set was used employing the generalized gradient approximation (GGA) method. The Perdew–Burke–Ernzerhof (PBE) was used for the exchange–correlation potential. The cutoff energy for the wave function expansion was set to 500 eV.